GEOLOGICA CARPATHICA, AUGUST 2022, 73, 4, 365–380 https://doi.org/10.31577/GeolCarp.73.4.5

Short Communication

Major and trace element signature of epidote-group minerals in altered pegmatites from the Petrovitsa Pb–Zn deposit of the Madan ore region, Central Rhodopes, Bulgaria: Evidence of allanite/epidote transformation

SYLVINA GEORGIEVA[1,✉], ROSSITSA VASSILEVA[1], GEORGI MILENKOV[1] and ELITSA STEFANOVA[1]

[1]Geological Institute, Bulgarian Academy of Sciences, "Acad. G. Bonchev" Str., bl. 24, 1113 Sofia, Bulgaria; ✉sylvina@geology.bas.bg

(Manuscript received May 9, 2022; accepted in revised form August 19, 2022; Associate Editor: Peter Bačík)

Abstract: The geochemical behaviour of major, rare, and trace elements in members of epidote-group minerals formed at different stages of magmatic and hydrothermal activity in pegmatites from the Madan ore district was studied. Accessory allanite-(Ce) and two generations of hydrothermal clinozoisite–epidote occur in hydrothermally-altered pegmatite bodies at the 820 mine level in the Petrovitsa Pb–Zn deposit. Abundant large concordant and crosscutting pegmatites (age 49.63 ± 0.94 Ma) with a thickness of more than 2 m are embedded in a high-grade metamorphic complex composed of various gneisses, amphibolites, and marbles in the area of the Petrovitsa deposit. The pegmatites consist mainly of feldspars and quartz, with plagioclases (albite–oligoclase, oligoclase–andesine, anorthite) predominating over K-feldspars. The main accessory minerals are allanite-(Ce), zircon, apatite, and an abundance of titanite. The overprinted hydrothermal mineral association is characterised by the formation of clinozoisite–epidote, adularia, chlorite, Ca-garnet, titanite, leucoxene, carbonates, hematite, and quartz. Based on petrographic observations, mineral relationships, and chemical properties, two generations of epidotes (*sensu lato*) were recognised: early epidote (Ep1) and late epidote (Ep2). Chemically, allanite-(Ce) contains high amounts of La and Th. The mineral suffered alteration due to several multiphase hydrothermal events and is partly or entirely transformed into REE-rich clinozoisite, causing depletion in REE and Th as well as enrichment of Si, Al, and Ca. The epidote 1 generation is defined chemically as clinozoisite to clinozoisite–epidote, whereas the late epidote 2 generation is clinozoisite–epidote, reaching epidote members. The REE contents in the studied epidotes from both generations are equally low with minor exceptions. The influx of later fluids percolated through and probably extracted REE from allanite and thereafter concentrated them in late-generation epidotes. This is also evidenced by some high REE contents in epidotes from both generations, formed in close proximity to allanite or titanite and/or overgrowing them, which is a sign of restricted REE transport.

Keywords: Pb–Zn deposits, hydrothermal alteration, pegmatite, allanite, epidote, clinozoisite

Introduction

Epidote-group minerals form during different geological processes, which leads to their occurrence in various metamorphic and igneous rocks, often being a product of metasomatic replacement. In pegmatites, they are frequently found as both primary magmatic accessory mineralisation and products of hydrothermal alteration of igneous minerals, such as feldspars, micas, etc. Allanite and epidote from altered pegmatite bodies in the Petrovitsa Pb–Zn deposit of the Madan ore region were studied in terms of mineral relationships and chemical composition. The studied minerals were formed during different stages of mineral-forming processes: as pegmatite accessories (allanite) and as a product of hydrothermal activity (clinozoisite–epidote solid solution).

The general formula of the epidote-group minerals is $A_2M_3[Si_2O_7][SiO_4](O,F)(OH,O)$, where the *A*-site is essentially occupied by Ca^{2+}, Mn^{2+}, Sr^{2+} or REE^{3+}, and *M*-site by Al^{3+}, Fe^{3+}or Mn^{3+}. The studied mineral species were determined according to the chemical substitutions in *A*- (REE^{3+}–Ca^{2+}) and *M*-octahedral positions (Al^{3+}–Fe^{3+}–Fe^{2+}) of the crystal structure (Armbruster et al. 2006).

This study focuses on the development, mineral relationships, and trace element signature of epidote-group minerals, which are represented both as accessory phases and as widespread hydrothermally-derived products in the altered pegmatites from the Petrovitsa Pb–Zn deposit.

Geological setting

The Madan ore district is located in the south-western part of the Central Rhodopes, South Bulgaria. Several Cenozoic (~30 Ma) Pb–Zn (±Ag) deposits, such as Petrovitsa, Krushev

Dol, Gjudjurska, Strashimir (Pechinsko pass), and others represent a significant Pb–Zn ore accumulation with great economic importance on a global scale (Vassileva et al. 2009 and references therein). The deposits are hosted by a high-grade metamorphic complex composed of various gneisses, minor amphibolite lenses or thin layers, and a number of marble lenses from the Madan Unit (Sarov et al. 2006) (Fig. 1). In the Petrovitsa deposit, abundant large concordant or crosscutting pegmatite bodies (>2 m wide) are regularly observed in the host rock assemblage representing two-mica and biotite gneisses and marbles. The main mineral composition of the gneisses is feldspars, quartz, micas, and chlorite. A typical texture of succession with melanocratic and leucocratic layers is observed.

The age of the pegmatite formation was determined by in-situ U–Pb geochronology on pegmatite-hosted titanite crystals as 49.63 ± 0.94 Ma (Milenkov et al. 2020). These pegmatite bodies, along with the host metamorphic rocks, suffered significant hydrothermal alteration prior to and during the ore deposition processes. An early stage of hydrothermal activity, which developed mainly along the lithological contact between pegmatites, marbles, and gneisses, led to the formation of distinct alteration in both aluminosilicate and carbonate environments. Manganese-rich skarns developed within the marbles composed of johannsenite–hedenbergite series and minor rhodonite. Under certain conditions and environment, bustamite forms, but it is not typical (Vassileva et al. 2009). In pegmatites and gneisses, the hydrothermal association is

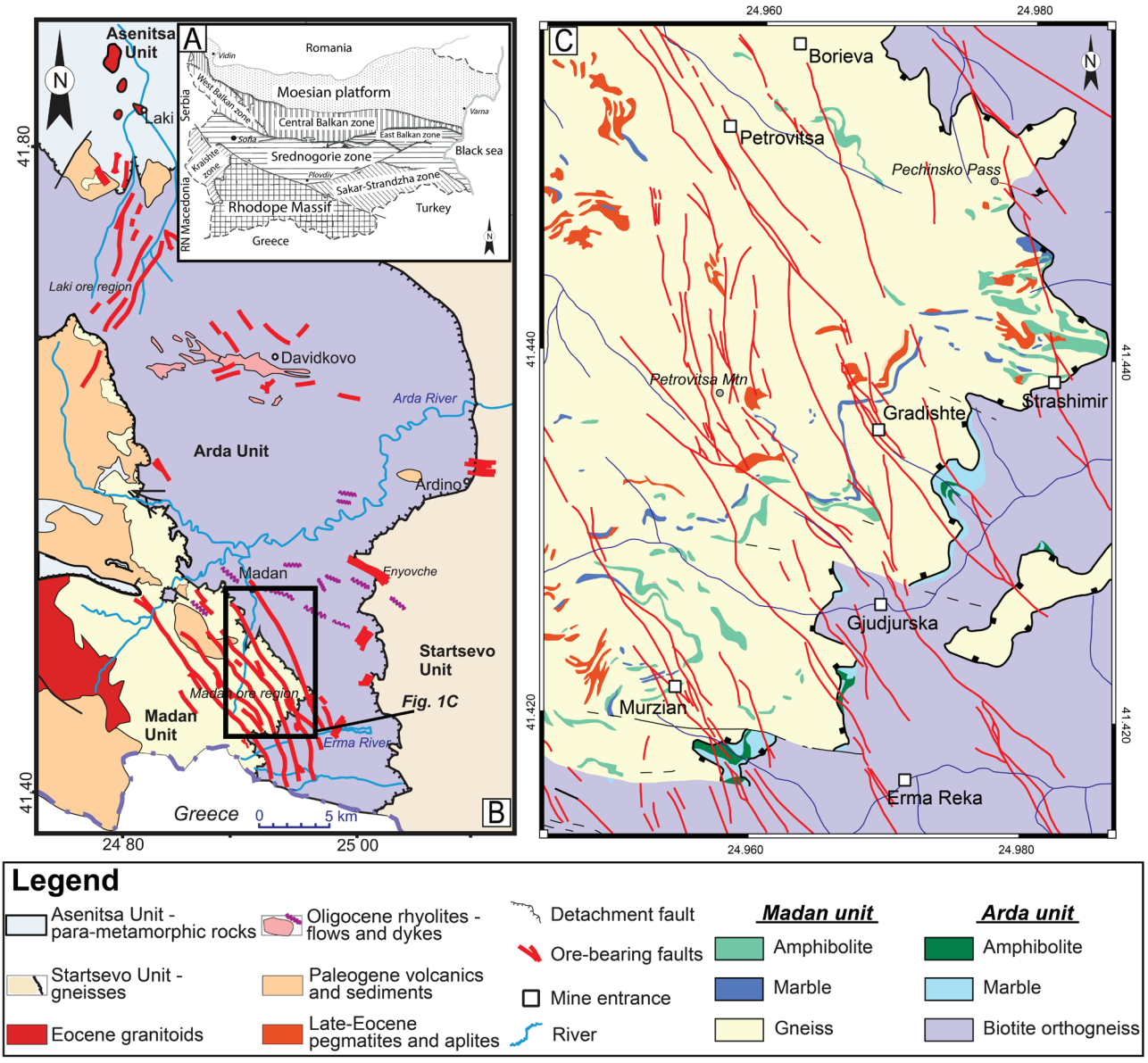

Fig. 1. A — Map of tectonic units of Bulgaria (modified from Ivanov 2017). **B** — Regional geological map of the Central Rhodopes and the main ore districts and deposits (Dimov et al. 2000; Vassileva et al. 2009). **C** — District-scale geological map with deposit locations (modified after Hantsche et al. 2021 and references therein).

composed mainly of epidote, K-feldspar, quartz, chlorite, sericite, carbonate, and titanite (Milenkov et al. 2022). The alteration is manifested mainly as a metasomatic replacement of feldspars. A late hydrothermal event related to the ore-forming processes in the deposit is marked by the formation of a second alteration assemblage. In pegmatites and gneisses, veinlets and nests composed of epidote, chlorite, quartz, K-feldspar, carbonate, Ca-garnet, sericite, clays, leucoxene (mixture of rutile and anatase), and hematite are developed. The retrograde mineral assemblage manifested by carbonate, quartz, rhodonite, bustamite, chlorite, and Mn-amphibole replaces the prograde skarns developed in marbles (Vassileva & Bonev 2003). The ore mineralisation in pegmatites is represented by scarce sphalerite and galena.

The morphology of the sulphide ore bodies in the deposit (galena–sphalerite±chalcopyrite) is pre-disponed by the properties of the host rocks and indicates two mechanisms of ore deposition along the sub-vertical NNW-oriented faults acting as a fluid conduit. In an aluminosilicate environment, the formation mechanism of the sub-vertical polymetallic veins is crystallisation in open space, while in a carbonate setting, a metasomatic replacement is favoured, and skarn-ore bodies are formed at the intersection with the marbles. The metallogenic source of the Madan deposits and the genetic link with a presumed magmatic intrusion have yet to be clarified, but it is important to note the presence of pegmatite bodies as major lithology in the depth of the Petrovitsa deposit.

Materials and analytical methods

Materials used in this study represent hydrothermally-altered samples from the pegmatite bodies of the Petrovitsa Pb–Zn deposit. Thin sections of representative samples were studied by optical microscopy in transmitted and reflected light, powder X-Ray Diffraction, scanning-electron microscopy with energy-dispersive X-ray spectroscopy (SEM-EDS), electron probe microanalyses (EPMA), and laser ablation with inductively-coupled plasma mass spectrometry (LA-ICP-MS). The epidote-group minerals association is determined by the XRD method, using Malvern Panalytical Multipurpose X-ray diffractometer Empyrean in the Laboratory of X-ray Diffraction Methods and Computed Tomography, Institute of Physical Chemistry, BAS. The minerals association relationships and the chemical composition were studied using JEOL JSM-6010PLUS/LA at the University of Mining and Geology. Major element compositions of the minerals were detected with EPMA JEOL 8200 Superprobe (University of Geneva), equipped with 5 wavelength-dispersive X-ray spectrometers (WDS). Accelerating voltage of 15 kV, beam current of 40 nA and a beam diameter of 2 μm were applied. Garnet (Y), La-phosphate (La), andalusite (Al), MnTi alloy (Ti), Ce-phosphate (Ce), forsterite (Mg), Th dioxide (Th), wollastonite (Si), MnTi alloy (Mn), Nd-phosphate (Nd), wollastonite (Ca), Ce-phosphate (P), albite (Na), orthoclase (K), and fayalite (Fe) were used as standards. The major elements were measured by K_α X-ray lines. The detection limits for elements in allanite expressed in ppm are: Si (105), Al (80), Ti (95), Ca (43), Fe (101), Mg (70), Mn (148), P (165), La (190), Ce (190), Nd (336), Th (122), and Y (1728). The detection limits for elements in epidote expressed in ppm are: Si (162), Al (111), Ti (135), Ca (68), Fe (138), Mg (134), Mn (168), Na (118), and K (58). The minor and trace element signature of the minerals was analysed by the LA-ICP-MS system in Geological Institute, BAS, consisting of New Wave Research (NWR) 193 nm Excimer laser UP-193FX attached to a Perkin-Elmer ELAN DRC-e quadrupole inductively coupled plasma mass spectrometer with 6 Hz and 25–50 μm.

The structural formulae of epidote-group minerals were calculated based on 12.5 oxygens and 8 cations. The Fe^{3+} was recalculated to the charge-balanced formula, based on the stoichiometric criteria proposed by Droop (1987). According to this recalculation, FeO in epidotes is absent.

Results

Mineral relationships

The mineral composition of the studied pegmatites represents mainly feldspars, quartz, and minor micas. The petrographic study showed that the quantity of quartz is about 20–30 % of the rock volume, and plagioclases prevail over K-feldspars (Vassileva et al. 2021). The main accessory minerals found in pegmatites are allanite, zircon, apatite, and an abundance of titanite. The geochemical properties of titanite were reviewed by Milenkov et al (2020). According to the profile sampling across a selected pegmatite body, the zonal distribution of the minerals shows the development of potassic feldspars ($Or_{69.8–97.2}$) in the central zones, together with some albite–oligoclase ($An_{0.8–26.8}$), giving way to oligoclase–andesine ($An_{30.9–36.5}$) in the intermediate zones; whereas along the contacts with the marbles, anorthite ($An_{89.4–100}$) is a major constituent. A clear hydrothermal alteration front is developed in the pegmatites, especially close to the lithological contacts. The overprinted hydrothermal mineral association is characterised by the formation of epidote-group minerals, adularia, chlorite ($X_{Fe}=0.30–0.46$; $X_{Mn}=0.01–0.18$), hematite, hydrothermal titanite, leucoxene, carbonates, and quartz (Georgieva et al. 2020, 2021) (Figs. 2, 3). Most often, the concentration of chlorite, titanite (altered later to leucoxene), and scarce clinopyroxene ($X_{Fe}=0.32–0.46$) are spatially related to the contacts of the pegmatite bodies with the gneisses and marbles, while epidote-group minerals, adularia, quartz, and carbonate regularly penetrate the inward volume of the altered pegmatites. In graphite-bearing marbles close to the contact of the altered pegmatite bodies, a narrow skarnization zone is observed (Fig. 2A, B). It is presented mainly by fine-fibrous radiating aggregates of bustamite alongside epidote. The association also includes late quartz and secondary manganoan carbonates.

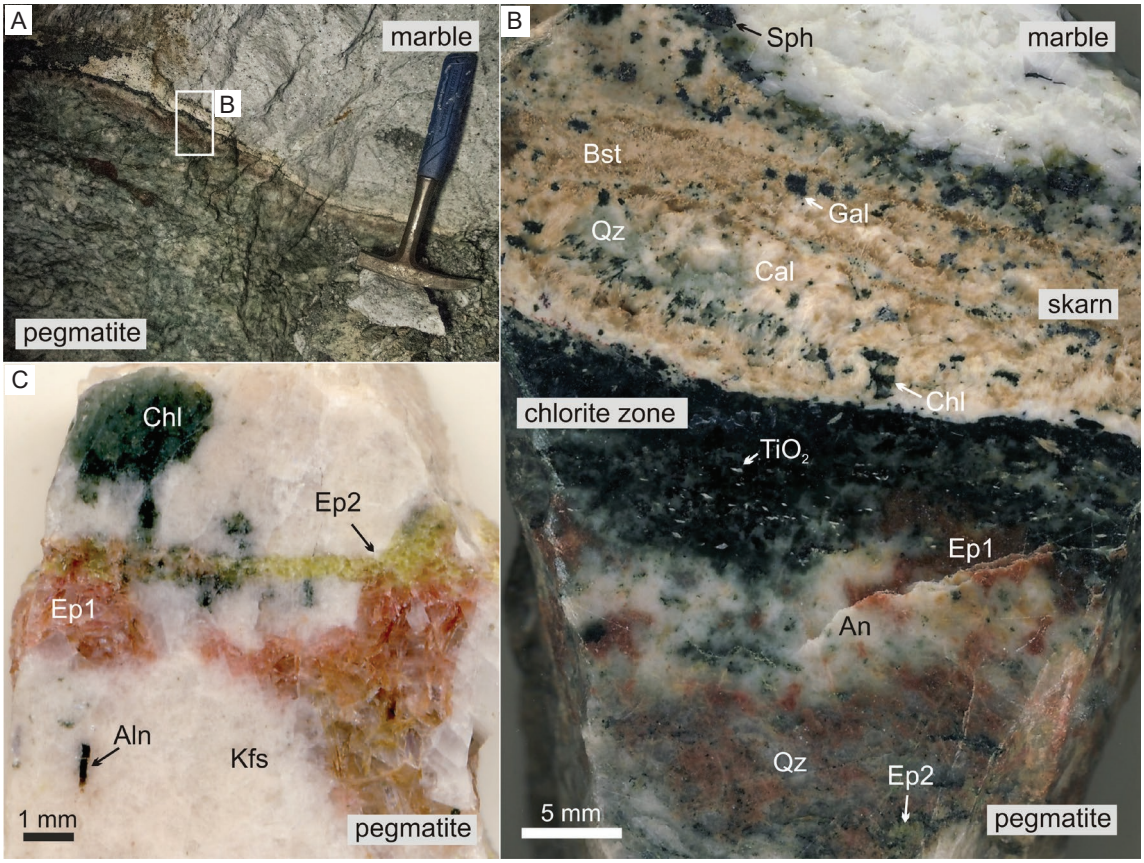

Fig. 2. Photographs of occurrence and mineral relationships in the epidote mineral association: **A** — Pegmatite-marble contact and position of the epidote alteration zone; **B** — Close view of the hydrothermal products after marble and pegmatite. Narrow skarnification zone with fine-fibrous radiating bustamite, quartz and secondary manganoan carbonates is observed within the marble close to the contact with the pegmatite; **C** — Occurrence and relationships of accessories allanite and the superimposed epidote 2 (green) generation over epidote 1 (pink) generation in pegmatite. Abb.: Ep – epidote; An – anorthite; Kfs – K-feldspar; All – allanite; Qz – quartz; Cal – calcite. Chl – chlorite; Bst – bustamite; Sph – sphalerite; Gal – galena.

The epidote-group minerals formed as a result of at least two distinct mineral-forming processes: (1) the early pegmatite injection with the formation of accessory allanite, and (2) later hydrothermal activity with the formation of two generations of epidote.

The accessory allanite typically forms up to 600 μm single euhedral crystals among grains of feldspar and/or quartz. Dark brown crystals up to 1 mm long are generally observed (Fig. 2C). Frequently, allanite crystals are overgrown on the periphery or fragmented and intersected by late hydrothermal epidote (Fig. 4A). Distinct zonal patterns in the mineral are visible in BSE images. Patchy or irregular zoning could be outlined in allanite, which rarely transforms into a distinct growth zoning in crystallographic continuity toward the periphery. In general, the outward growth zones are marked with traces of dissolution and recrystallisation (Fig. 4B–D). This footprint is suggested to be provoked by alteration of the primary mineral by late fluids penetrating through it.

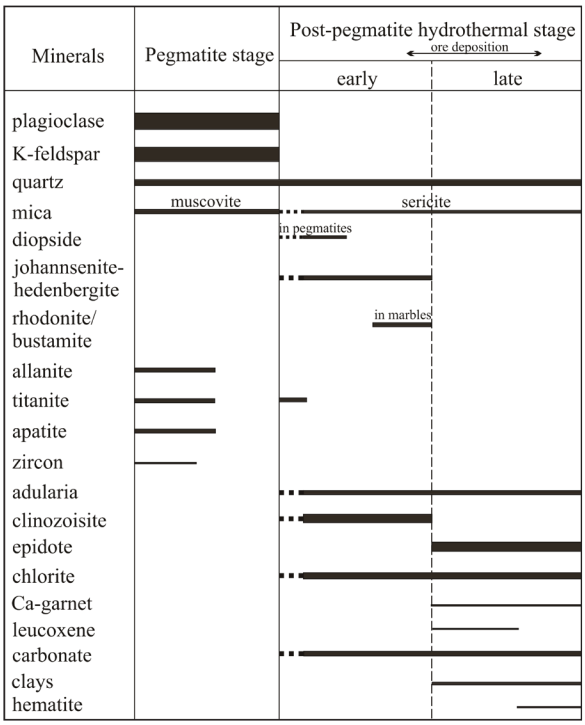

Fig. 3. Paragenetic table presenting mineral assemblage sequence in the Petrovitsa deposit.

Epidote represents one of the main products of the hydrothermal alteration developed in the Petrovitsa pegmatites. This is a result of multiphase mineral formation during the extensive hydrothermal activity in the region. Two generations of epidote can be distinguished in terms of textural relations and intersections among the mineral aggregates, morphology, colour, and chemistry. Both epidote generations are characterised by the incorporation of a small amount of Mn, which is a distinct geochemical feature for hydrothermal mineralisation in the region.

The early epidote generation (Ep1) is developed in pegmatites, as well as along their contact with graphite-bearing marbles, and generally occurs as sub- to euhedral prismatic (up to 1 cm) pale to deep pink or red single crystals or fine-crystalline clusters, forming radiating aggregates. The aggregates are developed in veins and nests, replacing coarse-grained pegmatite feldspars (anorthite, oligoclase-andesine, orthoclase) and intersecting quartz (Fig. 5A, B). The interstitial spaces among the epidote crystals are filled by calcite and quartz. The early epidote generation associates mainly with fine-grained chlorite, adularia (developed as single crystals or a fine network of veins and nests over feldspars), quartz, carbonate, accessory sub- to euhedral apatite, and euhedral titanite. The latter is subjected to hydrothermal dissolution and replacement by fine-crystalline leucoxene. The larger prismatic epidote crystals show clear zonal patterns on BSE images and EPMA due to the Al^{3+}/Fe^{3+} chemical heterogeneity (Fig. 5C, D). The cores of the crystals are generally dark reflecting the high Al content, whereas clear oscillatory zoning is observed toward the rim. Sectorial zoning is also frequently observed (Fig. 5E, F).

Epidote 1 (Ep1) mineralisation is usually overgrown or intersected by late epidote along with carbonate, chlorite, and quartz.

The second epidote generation (Ep2) is also spatially developed along the contact between pegmatite and marbles and penetrates into pegmatite volume. Epidote occurs mainly as anhedral pistachio green grains, forming nests and thin veinlets, and rarely as sub- to euhedral crystals (Fig. 6A–D). Except for the monomineral nests and veins formed in between feldspar and quartz, this later epidote is observed as a constituent of polymineral veins of quartz, chlorite, carbonate, and well-shaped clear adularia subhedral crystals (Fig. 6B). From

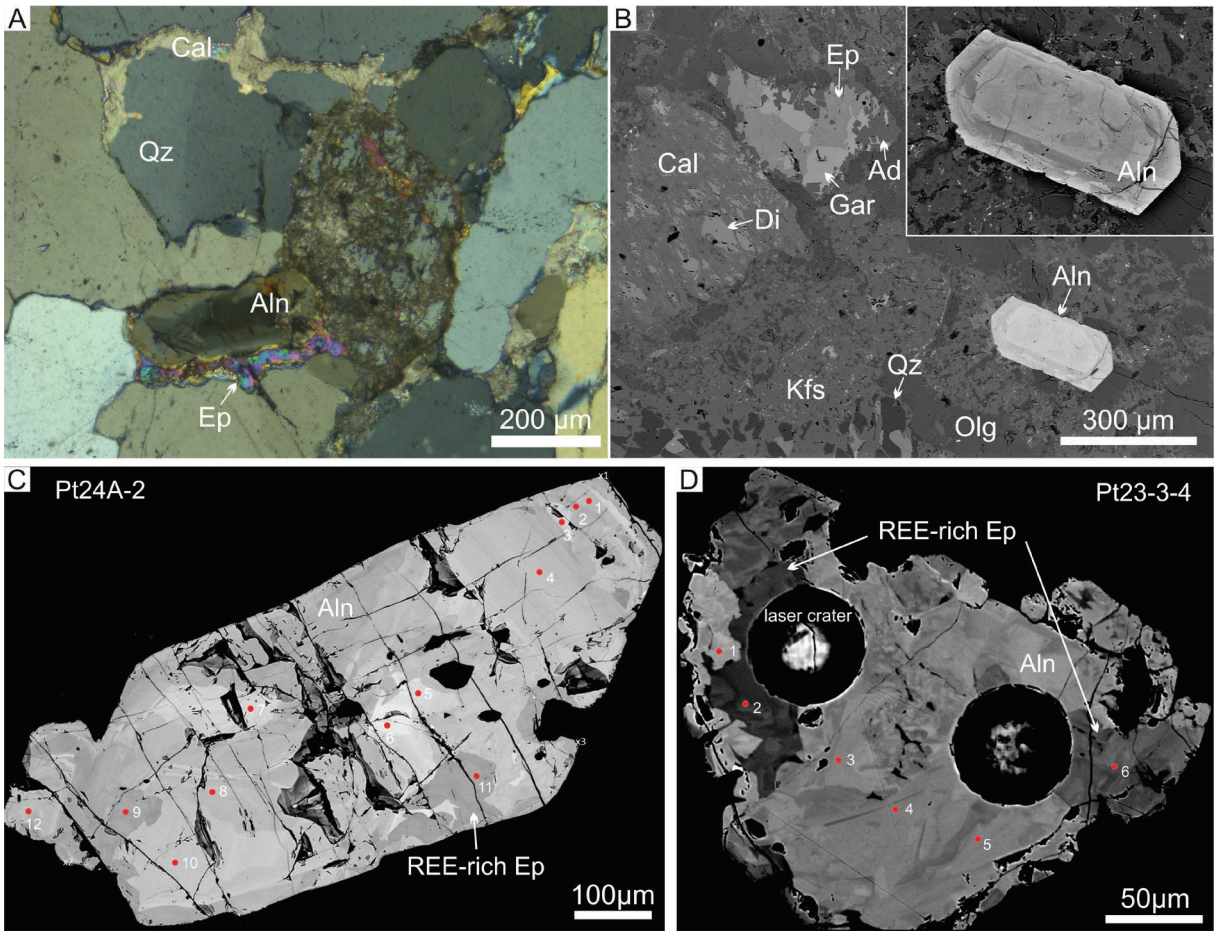

Fig. 4. Microphotographs of occurrence and mineral relationships of allanite: **A** — CPL image of allanite crystals overgrown on the periphery by late hydrothermal epidote; **B, C, D** — SEM-BSE image showing clear zonal patterns in the mineral. Irregular patchy domains are characteristic. The red circles show the locations of the EMP analyses. Abb.: Aln – allanite; Ep – epidote; Qz – quartz; Cal – calcite; Kfs – K-feldspar; Olg – oligoclase; Di – diopside; Gar – garnet; Ad – adularia. Red circles show some of the EPMA analyses locations.

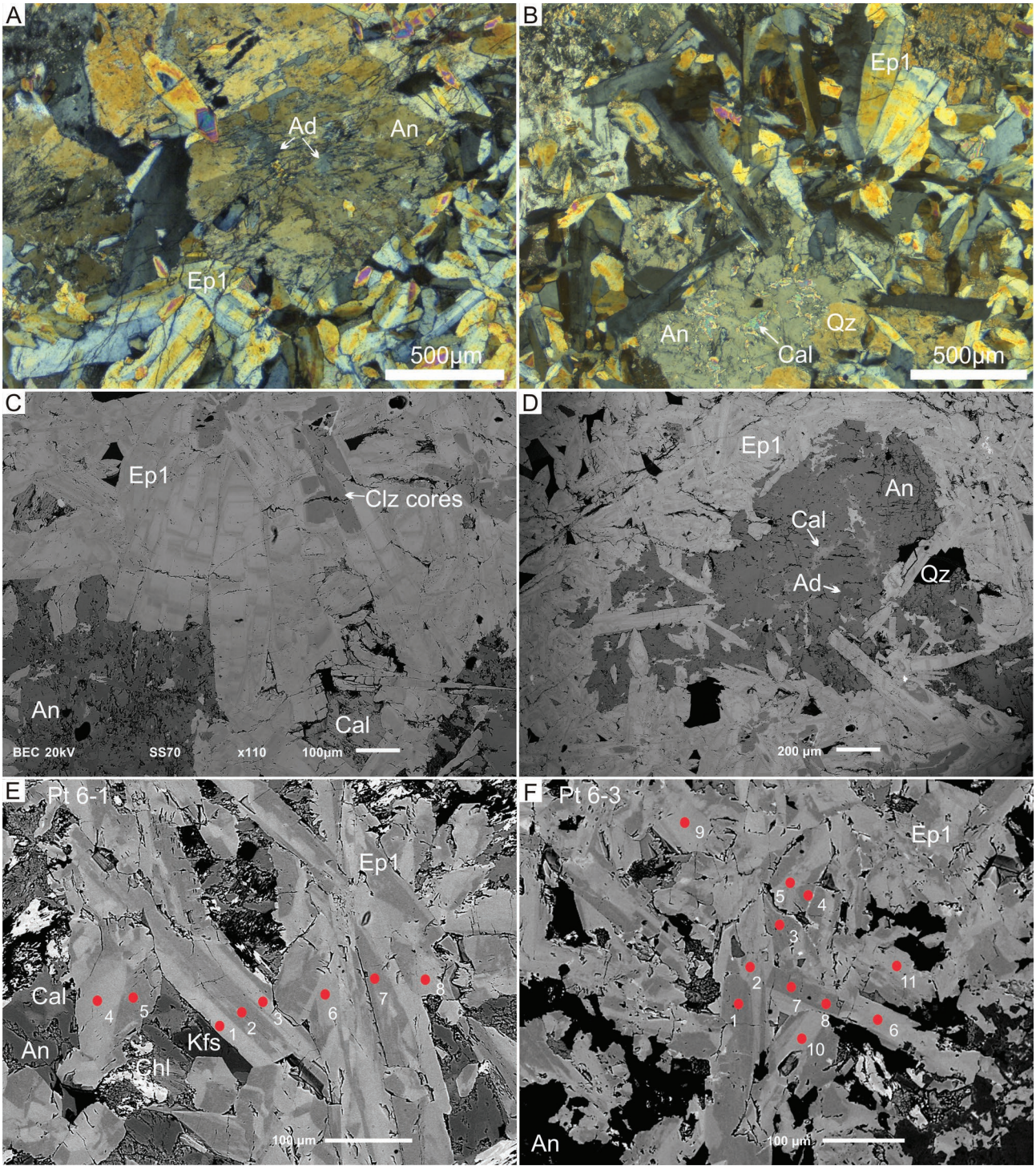

Fig. 5. Microphotographs of occurrence and mineral relationships of epidote 1 generation: **A, B** — CPL images of epidote prismatic crystals and their aggregates developed in veins and nests, replacing coarse-grained pegmatite feldspars (anorthite). Adularia and carbonate are developed in plagioclase; **C, D** — SEM-BSE images of zonal epidote crystal and aggregates. The chemical variation of Al^{3+}/Fe^{3+} in the crystals defines the zoning. The cores of the crystals are darker, reflecting the high Al content, whereas toward the periphery, clear oscillatory zoning is observed; **E, F** — SEM-BSE images showing different zonality and inhomogeneity in the mineral. The red circles show the locations of the EMP analyses. Abb.: Ep – epidote; Clz – clinozoisite; An – anorthite; Ad – adularia; Qz – quartz; Cal – calcite.

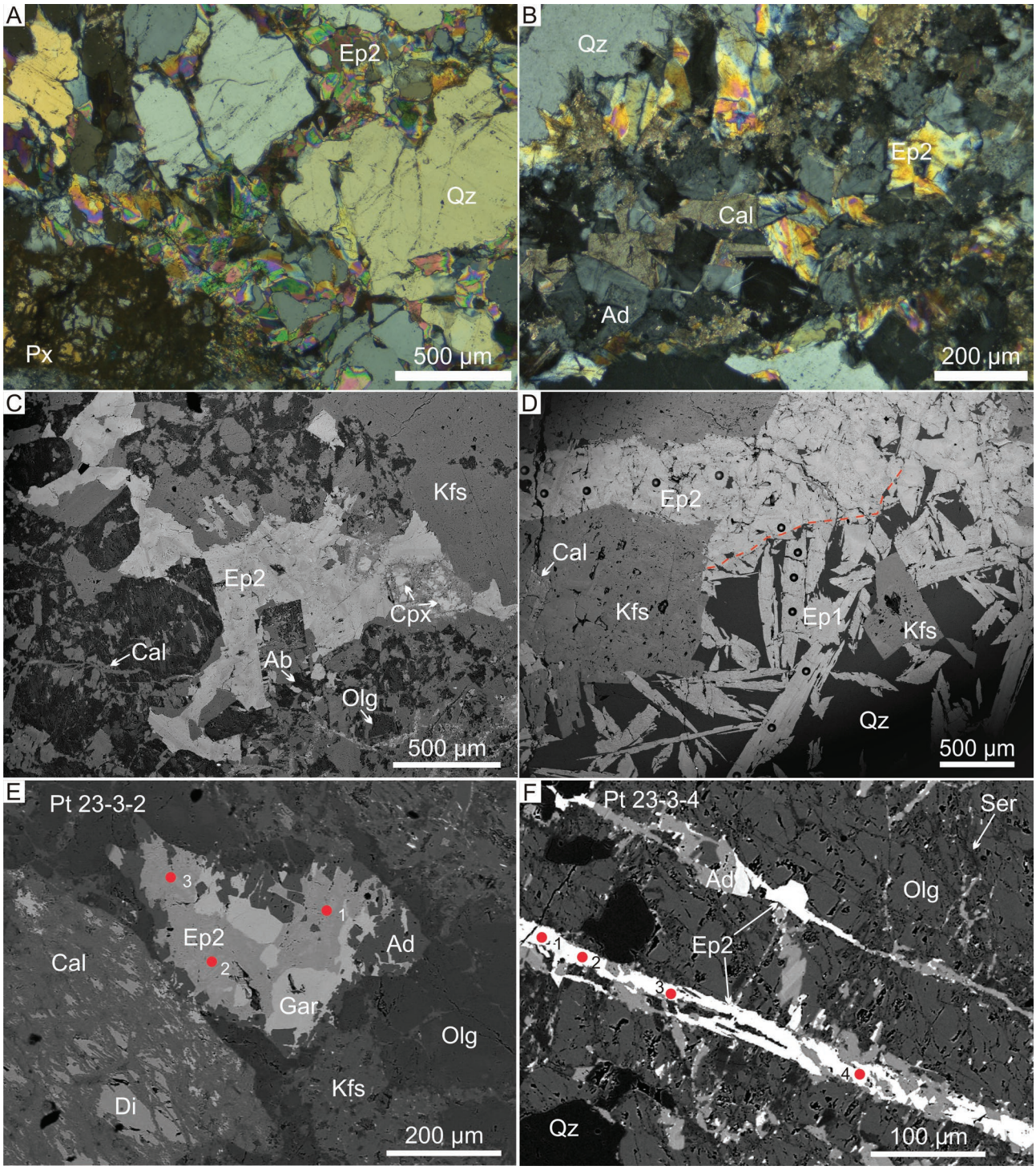

Fig. 6. Microphotographs of occurrence and mineral relationships of epidote 2 generation: **A** — CPL image of epidote anhedral grains and their aggregates developed in veins and nests; **B** — CPL image of polymineralic veins composed of epidote, chlorite, carbonate, and well-shaped clear adularia subhedral crystals; **C** — SEM-BSE images of zonal epidote with distinct heterogeneity without any clear pattern; **D** — SEM-BSE images of late epidote 2 generation, developed as anhedral grains intersecting early prismatic epidote 1 generation; **E** — SEM-BSE images of late epidote 2 generation in association with adularia and garnet; **F** — SEM-BSE images of late epidote 2 generation in association with adularia. The red circles show the locations of the EMP analyses. Abb.: Ep – epidote; Ad – adularia; Qz – quartz; Cal – calcite; Cpx – clinopyroxene; Kfs – K-feldspar; Olg – oligoclase; Ab – albite; Gar – garnet.

the periphery to the vein centre, a clear symmetric mineralogical sequence could be outlined: (epidote+calcite)–adularia –(epidote+calcite). Rare euhedral to subhedral Ca-garnet crystals are observed in the assemblage as well. Distinct heterogeneity is established in Ep2 grains based on SEM-BSE images without a clear pattern (Fig. 6C,D). This mineralisation intersects pegmatite feldspar and quartz, as well as the early formed Ep1 (see Fig. 6).

Chemical composition and tracing signatures

According to the chemical composition, the studied accessory mineral from the epidote group is predominantly allanite-(Ce) along with intermediate members of the isomorphous series with epidote and clinozoisite, reaching REE-rich clinozoisite (Fig. 7). The major REE in allanite is Ce, followed by La, Nd, Pr, Sm. High contents of Th, U, Y, and Cr are also established. The mineral contains stable low contents of MgO, TiO_2, MnO, P_2O_5, and traces of B, Sc, V, Cr, Co, Ni, Zn, Ga, Ge, As, Sr, Zr, In, Sn, Ba, Eu, Gd, Tb, Dy, Ho, Er, Tm, Yb, Lu, Hf, Pb, and Bi. The chemical composition of major, minor, and trace elements in allanite is summarised in Tables 1–3. A well-defined correlation between Ca and REE+Th+Y is observed (Fig. 8A). Among all measured elements, a relatively high content of V, Ga, and Ge should be noted. The amounts of the LREE (La, Ce, Pr, Nd, Sm) generally prevail over the HREE (Eu, Gd, Tb, Dy, Ho, Er, Tm, Yb, and Lu). A positive correlation between LREE and Th and HREE and Y can be observed due to their close chemical properties and ionic radii size (Fig. 8B,C). Chondrite-normalised patterns for REE in allanite display LREE>HREE and a distinct Eu anomaly corresponding to the general REE-characteristics in allanite from igneous rocks (Gieré & Sorensen 2004) (Fig. 8D). In cases of late hydrothermal alteration, its chemical composition shows a decrease in REE, Th, and Fe incorporations, whereas Al and Ca increase. This is related to a chemical exchange between primary allanite and hydrothermal fluids, provoking mobilisation and transport of REE+ACT and Fe during the fluid interaction and producing REE-poor altered allanite, reaching REE-rich clinozoisite.

According to the content of major elements, the studied hydrothermal epidotes from both generations are defined as members of the clinozoisite–epidote$_{ss}$, predominantly Fe^{3+}-rich clinozoisite towards epidote in the Ep2 generation (Armbruster et al. 2006). However, the composition of some major, minor, and trace elements through generations partly differ.

In Ep1, the content of CaO is within 21.79–24.5 wt%, Al_2O_3 is 23.56–29.53 wt% (with average values of 26.53 wt%), Fe_2O_3 ranges from 5.01–11.6 wt% (with average 8.59 wt%). The detected major, minor, and trace elements in this first-generation epidote are listed in Tables 1, 4, and 5. The mineral is characterised by a constant content of MnO, TiO_2, MgO and traces of B, V, Ga, Sr, Sb, and Pb. A negative correlation between Al and Fe contents is observed in the composition of the analysed crystals (Fig. 9A). The sum of Fe and Al is slightly lower and probably due to the presence of other elements in octahedral sites. On the other hand, in Fig. 9B, the sum of Ca and Mn is in excess and therefore, some of the Mn should be attributed to the *M*-site.

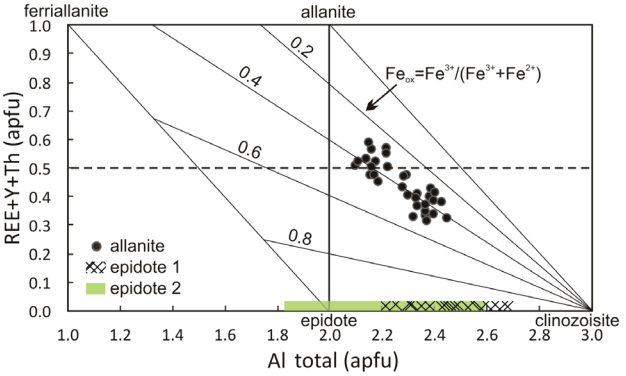

Fig. 7. Composition of epidote-group minerals represented by accessory allanite-(Ce), indicating alteration and transformation, and both clinozoisite–epidote generations from the Petrovitsa deposit represented on the classification diagram REE+Th+Y vs. Al (Petrík et al. 1995).

In general, the central parts of the studied mineral are enriched in Al, while in the rims, the Fe content augments. A wide variety of elements are detected in the predominant number of analyses with different magnitudes of concentration as Zn, Y, Nb, La, Ce, Eu, and U. Elements, such as Na, K, As, Rb, Zr, Ba, Pr, Nd, and Sm are a random constituent and do not show characteristic patterns. The last group of established elements such as Be, Sc, Cr, Co, Ni, Ge, Mo, Ag, In, Sn, Cs, Gd, Tb, Dy, Ho, Er, Tm, Yb, Lu, Hf, Ta, W, Bi, and Th are sporadically presented in single crystals or are below the detection limit. The content of Cr, Co, some REE, Th and U in Ep1 grains significantly increases on the contact or intersection zones with earlier allanite or titanite crystals.

The content of CaO in the studied Ep2 samples is similar to that in Ep1 (22.46–24.14 wt%). A slight decrease in Al_2O_3 (19.57–28.63 wt% and average values of 24.43 wt%) and an increase in Fe_2O_3 (6.14–17.99 wt% with average values of 11.68 wt%) are established compared to Ep1 (see Tables 1, 4, 5). A constant content of MnO, but relatively lower than in Ep1, MgO, TiO_2 and traces of B, V, Ga, Sr, Sb, and Pb are characteristic. The following elements: Zn, As, Y, Nb, Ba, La, Ce, Eu, and Bi are detected in the predominant number of analyses with different magnitudes of concentration. Randomly occurring elements without characteristic patterns are Na, Co, Ni, Ge, Rb, Nb, Cs, Pr, Nd, and U. Elements, such as K, Sc, Zr, Mo, Ag, In, Sn, Sm, Gd, Tb, Dy, Ho, Er, Tm, Yb, Lu, Hf, Ta, W, and Th are sporadically detected in single analyses or below the detection limit.

An increased content of Y and REE was found in thin epidote veinlets intersecting potassium feldspar and quartz in the border zone of the pegmatite. The presence of allanite or titanite in the examined area of the sample was not observed; however, their likely presence could be assumed considering the increased Y and REE values in the epidote.

Table 1: Major, minor and trace element represented as range of value of allanite – REE-rich clinozoisite and both generations epidotes (*sensu lato*) form the Petrovitsa deposit according to EPMA and LA-ICP-MS analyses.

	allanite, n=33				epidote 1 pink, n=57			epidote 2 green, n=50		
	min	max	average		min	max	average	min	max	average
SiO_2 wt%	33.44	36.25	35.00	SiO_2 wt%	37.97	39.26	38.67	37.27	39.36	38.33
TiO_2	0.15	0.55	0.30	TiO_2	0.00	0.15	0.02	0.00	0.07	0.01
Al_2O_3	19.54	24.63	22.07	Al_2O_3	23.56	29.53	26.53	19.57	28.63	24.43
FeO	5.85	10.10	7.88	Fe_2O_3	5.01	11.60	8.59	6.14	17.99	11.68
Fe_2O_3	0.10	2.19	0.85	MnO	0.00	2.47	0.65	0.00	1.76	0.23
MnO	0.00	0.33	0.06	MgO	0.00	0.09	0.01	0.00	0.15	0.02
MgO	0.18	1.12	0.56	CaO	21.79	24.50	23.59	22.46	24.14	23.70
CaO	12.84	18.15	15.79	Na_2O	0.00	0.03	0.00	0.00	0.03	0.00
Y_2O_3	0.00	0.89	0.22	K_2O	0.00	0.03	0.00	0.00	0.10	0.01
La_2O_3	2.60	4.15	3.37	P_2O_5	0.01	0.03	0.02	0.01	0.03	0.02
Ce_2O_3	4.94	8.59	6.77	Li ppm	<0.48	7.88	4.15	<0.43	8.81	3.65
Nd_2O_3	1.30	3.34	2.18	Be	<3.09	63.72	24.02	<3.10	75.36	22.77
ThO_2	1.17	3.68	1.82	B	17.58	86.60	39.05	11.29	110.75	39.69
P_2O_5	0.07	0.16	0.12	Sc	<1.74	6.34	3.35	<1.77	5.46	3.11
Li ppm	<1.89	5.56	3.37	V	1.69	121.04	29.91	1.99	91.56	29.38
Be	<2.36	19.78	6.04	Cr	<14.26	33.74	22.69	<10.89	36.56	21.96
B	11.82	31.52	21.20	Co	<0.33	5.14	1.19	<0.72	12.94	1.73
Sc	32.69	67.07	39.78	Ni	<4.99	36.86	20.05	<5.56	49.34	20.84
V	329.45	769.43	600.53	Cu	<0.56	<6.06	<3.73	<2.17	5.39	3.54
Cr	1214.83	5475.14	3965.38	Zn	5.60	37.13	13.48	5.28	33.03	15.14
Co	6.19	10.84	8.83	Ga	21.33	169.24	47.54	27.18	103.34	68.19
Ni	20.63	71.02	44.68	Ge	<2.36	16.09	9.75	<3.39	16.21	9.08
Cu	<0.79	5.09	2.60	As	<3.30	25.81	8.83	<4.87	62.28	13.66
Zn	118.76	177.88	139.67	Rb	<0.07	3.45	0.59	<0.24	10.53	1.51
Ga	609.74	903.63	787.52	Sr	686.31	1945.86	1219.41	733.85	2665.81	1437.61
Ge	503.62	768.48	667.11	Y	0.06	10.36	2.36	0.06	32.75	2.48
As	73.80	102.44	84.86	Zr	<0.13	5.42	1.13	<0.10	0.94	0.45
Rb	<0.21	4.52	0.62	Nb	<0.07	5.47	1.10	<0.07	1.83	0.45
Sr	159.32	293.79	211.72	Mo	<0.45	4.29	2.39	<0.44	<3.99	<1.89
Zr	7.36	14.89	10.86	Ag	<0.14	1.35	0.73	<0.18	0.48	0.73
Nb	<0.05	0.42	0.18	Cd	<0.93	8.05	4.50	<0.94	<8.42	<4.87
Mo	<0.34	2.60	1.31	In	<0.04	0.61	0.22	<0.05	0.44	0.22
Ag	<0.13	0.58	0.30	Sn	<0.63	2.40	1.30	<0.32	6.69	1.56
Cd	<2.01	5.18	3.57	Sb	1.79	43.43	9.63	1.06	20.28	7.37
In	1.24	2.88	2.11	Cs	<0.04	1.42	0.24	<0.04	4.37	0.56
Sn	5.46	18.87	14.93	Ba	<0.39	11.37	2.25	<0.38	15.04	3.04
Sb	<0.15	11.64	1.31	La	<0.04	0.98	0.31	<0.05	11.58	1.17
Cs	<0.03	0.45	0.13	Ce	<0.06	3.16	0.59	<0.05	25.34	2.32
Ba	0.68	22.63	2.89	Pr	<0.04	0.54	0.20	<0.04	3.77	0.38
Pr	2192.55	4956.17	3849.02	Nd	<0.20	2.33	1.11	<0.25	17.04	1.91
Sm	937.06	1967.50	1461.39	Sm	<0.23	2.43	1.16	<0.29	3.97	1.12
Eu	47.93	128.20	86.17	Eu	<0.06	2.15	0.60	<0.11	5.97	0.99
Gd	538.08	1057.31	760.22	Gd	<0.25	2.43	1.13	<0.32	5.05	1.16
Tb	48.07	103.73	62.08	Tb	<0.04	0.36	0.17	<0.05	0.63	0.18
Dy	150.16	402.74	214.64	Dy	<0.16	1.74	0.87	<0.19	5.80	1.02
Ho	18.72	60.45	27.98	Ho	<0.04	0.51	0.19	<0.05	1.17	0.23
Er	33.78	124.39	53.75	Er	<0.18	2.34	0.79	<0.21	4.48	0.86
Tm	3.34	12.16	5.21	Tm	<0.04	0.36	0.17	<0.05	0.71	0.19
Yb	16.57	57.20	28.02	Yb	<0.23	2.12	0.96	<0.31	5.11	1.23
Lu	2.03	7.38	3.64	Lu	<0.04	0.36	0.16	<0.05	0.60	0.17
Hf	0.53	1.96	1.10	Hf	<0.15	1.21	0.64	<0.17	1.12	0.52
Ta	<0.05	0.28	0.15	Ta	<0.06	1.15	0.33	<0.05	0.52	0.20
W	<0.23	5.79	0.77	W	<0.22	2.31	1.00	<0.28	12.27	1.51
Pb	33.58	91.45	65.44	Pb	4.74	49.56	21.82	4.78	43.42	21.34
Bi	0.32	3.14	1.19	Bi	<0.05	4.05	0.51	<0.31	3.85	1.01
U	403.68	1676.17	1166.77	Th	<0.03	0.44	0.17	<0.05	0.44	0.15
				U	0.11	1.53	0.62	<0.05	2.57	0.44

Table 2: EPMA representative analyses of allanite – REE-rich clinozoisite from the Petrovitsa deposit (wt%).

Type	allanite – REE-rich clinozoisite											
Sample	Pt-23-3-1-1	Pt-23-3-1-3	Pt-23-3-1-4	Pt-24A-2-1	Pt-24A-2-2	Pt-24A-2-5	Pt-24A-2-6	Pt-24A-2-7	Pt-24A-2-8	Pt-24A-2-9	Pt-24A-2-10	Pt-24A-2-11
Details	crystal 1			crystal 2								
	corroded rim	centre	corroded rim	rim	rim	centre	centre	centre	centre	corroded rim	rim	corroded rim
SiO_2	36.07	35.60	36.02	33.74	34.08	33.71	33.44	33.92	34.27	34.43	33.97	34.65
TiO_2	0.19	0.23	0.18	0.49	0.46	0.30	0.31	0.55	0.24	0.40	0.29	0.42
Al_2O_3	23.83	23.60	23.54	20.00	20.18	19.99	19.85	19.65	20.99	20.55	20.79	20.86
FeO	6.99	6.58	6.78	8.99	9.02	9.95	10.10	9.96	9.39	8.94	9.42	8.75
Fe_2O_3	0.75		1.32	1.34	1.20			0.28		1.21		1.39
MnO	0.00	0.00	0.00	0.15	0.19	0.33	0.29	0.10	0.21	0.03	0.18	0.02
MgO	0.29	1.12	0.21	0.52	0.53	0.66	0.69	0.56	0.72	0.43	0.71	0.40
CaO	17.50	16.26	17.69	14.19	14.36	12.93	12.84	14.08	13.54	14.91	13.43	15.32
P_2O_5	0.10	0.14	0.10	0.14	0.10	0.12	0.11	0.09	0.10	0.12	0.15	0.12
Y_2O_3	0.00	0.29	0.19	0.49	0.53	0.88	0.68	0.05	0.89	0.07	0.32	0.01
La_2O_3	2.83	3.53	2.74	3.67	2.60	3.18	3.56	3.88	3.68	3.16	3.59	3.20
Ce_2O_3	5.25	6.65	5.18	8.08	6.83	7.72	8.46	7.56	8.59	7.51	8.45	7.04
Nd_2O_3	1.73	1.91	1.64	2.80	3.34	3.33	3.32	1.98	3.06	2.82	3.25	2.46
ThO_2	1.65	1.93	1.50	1.48	1.48	2.24	2.15	3.68	1.34	1.59	1.55	1.99
Total	97.17	97.84	97.10	96.08	94.90	95.34	95.80	96.33	97.01	96.17	96.09	96.62
apfu												
Si	3.072	3.050	3.070	3.055	3.086	3.089	3.072	3.088	3.070	3.081	3.071	3.075
P	0.007	0.010	0.007	0.010	0.007	0.009	0.009	0.007	0.007	0.009	0.011	0.009
Σ T	3.079	3.060	3.078	3.066	3.093	3.098	3.081	3.095	3.077	3.090	3.083	3.084
Ti	0.012	0.015	0.012	0.033	0.031	0.021	0.021	0.037	0.016	0.027	0.020	0.028
Al	2.392	2.383	2.365	2.135	2.154	2.159	2.149	2.108	2.216	2.167	2.215	2.182
Fe^{2+}	0.498	0.459	0.483	0.671	0.662	0.729	0.735	0.758	0.672	0.667	0.669	0.644
Fe^{3+}	0.048		0.085	0.091	0.082			0.019		0.082		0.093
Mg	0.036	0.143	0.027	0.070	0.071	0.091	0.095	0.075	0.096	0.057	0.096	0.053
Σ M	2.986	3.000	2.971	3.000	3.000	3.000	3.000	2.999	3.000	3.000	3.000	3.000
Fe^{2+}		0.012		0.010	0.021	0.033	0.041		0.032	0.002	0.043	0.006
Mn	0.000	0.000	0.000	0.012	0.015	0.026	0.022	0.008	0.016	0.002	0.014	0.001
Ca	1.597	1.493	1.616	1.377	1.393	1.269	1.264	1.373	1.300	1.429	1.301	1.457
Y	0.000	0.013	0.009	0.024	0.026	0.043	0.033	0.002	0.042	0.003	0.015	0.000
La	0.089	0.112	0.086	0.123	0.087	0.107	0.121	0.130	0.122	0.104	0.120	0.105
Ce	0.164	0.209	0.162	0.268	0.226	0.259	0.285	0.252	0.282	0.246	0.280	0.229
Nd	0.053	0.059	0.050	0.091	0.108	0.109	0.109	0.064	0.098	0.090	0.105	0.078
Th	0.032	0.038	0.029	0.030	0.030	0.047	0.045	0.076	0.027	0.032	0.032	0.040
Σ A	1.934	1.934	1.951	1.934	1.907	1.893	1.920	1.907	1.918	1.910	1.909	1.916
REE+ACT	0.337	0.429	0.336	0.535	0.478	0.565	0.592	0.525	0.571	0.476	0.552	0.452

Chemically, both epidote generations are defined as members of the clinozoisite–epidote$_{ss}$, presented predominantly by Fe^{3+}-rich clinozoisite. With the Fe increase in the fluid, epidote end members with Fe_2O_3 composition of 16.32–17.99 wt% or 1–1.1 *apfu* are established in later Ep2 generation. As a rule, Ep1 expressed high Al-content, and the central parts of the grains are generally enriched in Al compared to the periphery, where Fe augment. The first generation is characterised by a relatively higher Mn content compared to the Ep2; however, even in small amounts (up to 0.16 *apfu*), it is sufficient to act as a chromophore and give a pink colouring, despite the presence of the iron content. Both epidote generations do not reveal a high concentration of REE, although Ep2 demonstrates relatively higher REE incorporation (Fig. 10). Comparatively increased REE contents were established only in crystals and grains grown close to the previously formed accessories (allanite and titanite). At the same time, the REE depletion in accessory minerals is documented.

Discussion

The studied epidote-group minerals in altered pegmatite from the Petrovitsa deposit formed during temporally different mineral-forming processes – allanite as the primary pegmatite accessory mineral, while both epidote generations result from late hydrothermal alteration.

According to the recommended nomenclature of epidote-group minerals by Armbruster et al. (2006), the approved chemical criterion to assign minerals to the allanite subgroup

Table 3: LA-ICP-MS representative analyses of allanite – REE-rich clinozoisite from the Petrovitsa deposit (ppm).

Type	allanite – REE-rich clinozoisite												
Sample	Cl23 11	Cl23 3	Cl23 4	Cl23 5	Cl23 6	Cl23 10	Cl23 7	Cl23 8	23-3 17	23-3 18	23-3 19	23-3 10	23-3 11
Details	crystal 1								crystal 2			crystal 3	
	profile								centre	middle	rim	centre	rim
Li	1.89	bdl	bdl	2.57	2.32	2.70	2.59	2.69	bdl	4.85	bdl	bdl	bdl
B	17.49	18.51	27.85	24.40	26.40	12.30	20.29	22.24	21.70	27.75	17.31	20.50	11.82
Sc	36.13	33.33	33.64	33.09	33.94	38.19	32.69	35.08	39.66	43.93	37.68	48.54	53.96
V	725.85	692.29	724.61	729.38	700.24	716.17	686.00	710.98	541.63	541.73	443.04	769.43	706.93
Cr	5031.73	4806.79	4925.04	4942.43	4866.80	5475.14	4818.38	4850.23	2589.33	3629.25	4206.87	4501.64	4107.59
Co	9.01	8.09	10.84	9.60	9.38	8.16	8.59	9.12	7.79	6.19	9.75	9.49	9.27
Ni	22.54	29.39	54.57	36.99	29.72	20.63	33.80	49.62	42.94	35.39	64.83	36.51	51.29
Zn	145.65	140.71	148.38	129.28	135.31	145.88	132.66	138.08	120.90	118.76	119.00	156.47	139.49
Ga	845.68	844.50	833.88	894.21	844.73	860.48	826.93	903.63	745.11	713.26	609.74	888.00	863.65
Ge	736.39	731.48	768.48	766.03	718.80	691.69	684.62	734.71	632.71	638.61	508.75	768.12	766.31
As	90.93	91.76	87.71	84.90	83.73	86.96	84.51	93.12	74.83	80.42	73.80	102.44	98.79
Sr	200.38	176.75	172.36	172.17	278.97	173.44	182.49	204.78	278.20	276.56	293.79	159.32	176.77
Y	526.25	553.68	710.05	540.49	570.64	615.85	495.90	572.77	518.01	717.99	1084.79	717.47	791.81
Zr	8.33	9.33	12.16	8.89	9.15	9.94	7.36	8.34	9.69	11.20	14.89	8.89	12.23
In	2.11	2.53	1.96	2.25	2.19	2.23	2.28	2.12	1.24	1.64	2.88	2.15	2.20
Sn	16.09	18.87	17.87	15.97	18.61	18.27	16.26	17.16	5.46	7.30	16.08	14.77	16.25
Ba	0.97	bdl	bdl	2.88	22.63	0.68	2.20	0.81	1.94	1.45	3.89	1.04	1.72
La	24244.4	27152.8	27034.8	27603.0	26159.1	23680.1	26272.4	28428.4	22089.2	20321.7	16748.2	25831.4	24133.5
Ce	44288.1	50542.6	51712.6	54160.1	51139.3	43312.0	51394.7	55836.6	41986.5	40032.5	31414.2	49085.4	46877.5
Pr	4173.2	4065.9	4062.9	4230.0	4005.3	4103.9	4038.2	4307.6	4017.7	3942.6	3157.3	4956.2	4694.5
Nd	13057.1	12819.9	13133.5	12727.9	12298.6	12931.8	12296.5	13091.9	12582.9	12950.1	10345.1	16724.0	15701.8
Sm	1453.8	1455.2	1604.7	1469.6	1448.8	1515.0	1344.2	1463.6	1276.6	1513.0	1342.2	1967.5	1876.0
Eu	74.21	84.21	85.09	77.96	76.69	80.91	75.78	81.18	94.99	111.54	128.20	84.91	87.23
Gd	707.10	706.36	806.72	712.90	728.08	766.05	640.70	677.80	648.21	795.71	809.41	1004.66	976.06
Tb	52.13	53.16	62.30	50.77	53.85	59.31	48.26	53.26	50.00	66.62	72.96	77.07	76.81
Dy	164.78	172.24	219.36	166.38	179.18	184.07	150.16	173.22	169.81	240.72	288.29	231.12	248.37
Ho	20.08	21.13	27.98	20.40	21.62	23.10	18.72	23.18	20.52	29.93	40.97	27.31	29.98
Er	36.49	37.26	50.56	39.04	40.22	43.80	33.78	39.32	39.77	55.98	83.76	50.77	54.04
Tm	3.66	3.81	5.47	3.63	3.84	4.16	3.34	4.16	3.54	4.99	7.49	4.62	4.98
Yb	21.66	22.32	23.02	22.49	24.11	27.30	18.94	22.46	16.57	22.52	44.74	24.43	32.12
Lu	2.84	3.23	3.82	2.82	3.04	3.50	2.99	3.22	2.03	2.69	5.29	3.78	4.30
Hf	0.88	1.41	0.53	0.90	0.72	0.93	1.16	1.80	0.77	1.02	1.51	1.14	1.05
Pb	69.12	68.56	90.95	70.92	91.45	72.45	62.99	70.22	67.68	76.47	66.10	61.60	55.34
Bi	0.55	0.85	0.90	0.71	1.11	0.90	0.72	0.70	2.30	3.14	2.62	0.62	0.88
Th	13327.4	12624.3	25663.8	12644.5	24873.6	13595.3	11691.2	12342.1	10063.1	11477.8	10215.4	13002.8	11602.3
U	1097.4	1159.6	1457.6	1181.3	1306.5	1240.3	988.6	1255.8	403.7	599.3	1676.2	1162.5	1143.4

is REE+ACT>0.5 *apfu.* The obtained chemical data for allanite from the Petrovitsa deposit indicate REE+ACT contents in the range between 0.31–0.59 *apfu*. This fact, as well as the increased values of Al, Si, and Ca in the majority of the analyses, suggests hydrothermal alteration of allanite. The processes of leaching and migration of REE during fluid-mineral interaction results in a chemical variation of the mineral and correspond to the allanite/epidote transformation proposed by Poitrasson (2002). The REE enrichment of the late epidote formation on or close to allanite crystals indicates very short transport of the REE (as also suggested by Gros et al. 2020).

The studied allanite is determined as a Ce-dominant member with the incorporation of La, Th, Nd, Y, Cr, V, Ga, and Ge. The most probable mechanism of trivalent REE and Y incorporation into the *A*-site of the crystal structure is the replacement via polyvalent substitution: Ca^{2+} is replaced by REE^{3+} at *A*-sites, coupled with the substitution of divalent for trivalent cations in the *M*-sites in order to maintain the charge balance (Dollase 1971; Peterson & MacFarlane 1993; Frei et al. 2004; Gieré & Sorensen 2004; Armbruster et al. 2006; Bačík & Uher 2010):

$Ca^{2+}+Fe^{3+}\rightarrow REE^{3+}+Fe^{2+}$ for epidote,

$Ca^{2+}+Al^{3+}\rightarrow REE^{3+}+Fe^{2+}$ for clinozoisite,

or ${}^{A2}Ca^{2+}+{}^{M3}M^{3+}\rightarrow {}^{A2}REE^{3+}+{}^{M3}M^{2+}$,

where M^{3+} represents Al^{3+} and Fe^{3+}, and M^{2+} can contain Fe^{2+}, Mg^{2+} and Mn^{2+}.

The incorporation of Mg^{2+} at *M*-sites of the allanite crystal structure is likely favoured by the same mechanism. Assuming the higher redox potential of Mn, the presence of Mn^{2+} rather

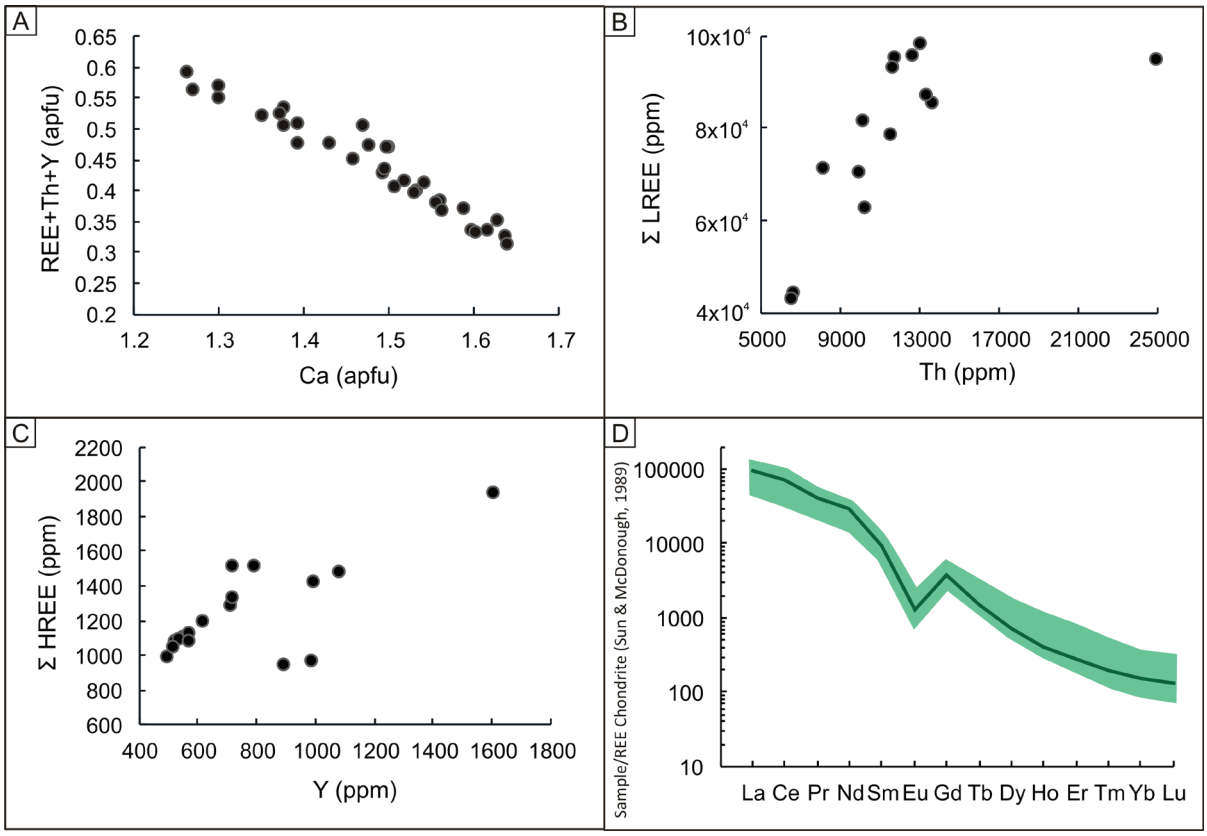

Fig. 8. Correlation diagrams in allanite between Ca and REE+Th+Y (**A**), LREE and Th (**B**), HREE and Y (**C**). **D** — Chondrite-normalised REE patterns (normalisation values after Sun & McDonough 1989); the shaded fields indicate range of values.

Table 4: EPMA representative analyses of both epidotes generations from the Petrovitsa deposit (wt%).

Type	**epidote 1 pink**						**epidote 2 green**				
Sample	**Pt-6-1-1**	**Pt-6-1-2**	**Pt-6-1-3**	**Pt-6-3-7**	**Pt-6-3-8**	**Pt-6-3-6**	**Pt-23-3-2-1**	**Pt-23-3-2-2**	**Pt-23-3-2-3**	**Pt-23-3-4-3**	**Pt-23-3-4-4**
Details	**crystal 1**			**crystal 2**							
	rim	**core**	**rim**	**core**	**core**	**rim**	**nest**	**nest**	**nest**	**veinlet**	**veinlet**
SiO_2	38.89	38.96	38.85	38.98	39.09	38.47	37.65	37.63	37.72	37.76	38.27
Al_2O_3	25.51	28.25	26.30	28.78	28.42	25.73	21.22	19.57	20.10	22.56	22.41
TiO_2	0.00	0.00	0.00	0.02	0.04	0.02	0.00	0.00	0.02	0.00	0.00
Fe_2O_3	10.07	6.54	8.87	6.37	6.57	10.12	15.62	17.99	16.32	12.98	13.41
MgO	0.00	0.00	0.00	0.00	0.00	0.00	0.04	0.03	0.09	0.15	0.11
MnO	0.04	0.06	0.06	0.05	0.06	0.04	0.08	0.05	0.10	0.08	0.07
CaO	24.00	24.26	24.21	24.33	24.33	23.97	23.27	23.09	23.04	23.79	23.66
Na_2O	0.00	0.00	0.00	0.02	0.00	0.00	0.00	0.00	0.00	0.00	0.00
K_2O	0.01	0.00	0.00	0.00	0.00	0.00	0.02	0.01	0.01	0.04	0.10
Total	98.52	98.07	98.29	98.55	98.50	98.35	97.90	98.37	97.41	97.35	98.03
apfu											
Si (T)	3.041	3.019	3.032	3.002	3.016	3.012	3.027	3.038	3.059	3.022	3.047
Al	2.351	2.580	2.419	2.612	2.584	2.375	2.010	1.863	1.921	2.128	2.103
Ti	0.000	0.000	0.000	0.001	0.002	0.001	0.000	0.000	0.001	0.000	0.000
Fe^{3+}	0.593	0.382	0.521	0.370	0.382	0.597	0.946	1.094	0.997	0.783	0.804
Mg	0.000	0.000	0.000	0.000	0.000	0.000	0.005	0.003	0.010	0.018	0.013
Mn	0.003	0.004	0.004	0.003	0.004	0.002	0.005	0.003	0.007	0.005	0.005
Σ M	2.944	2.962	2.940	2.983	2.969	2.974	2.962	2.960	2.931	2.929	2.920
Ca	2.011	2.015	2.024	2.008	2.012	2.011	2.004	1.997	2.002	2.040	2.018
Na	0.000	0.000	0.000	0.004	0.000	0.000	0.000	0.000	0.000	0.000	0.000
K	0.001	0.000	0.000	0.000	0.000	0.000	0.002	0.002	0.002	0.004	0.010
Σ A	2.012	2.015	2.024	2.012	2.012	2.011	2.006	1.999	2.004	2.044	2.028

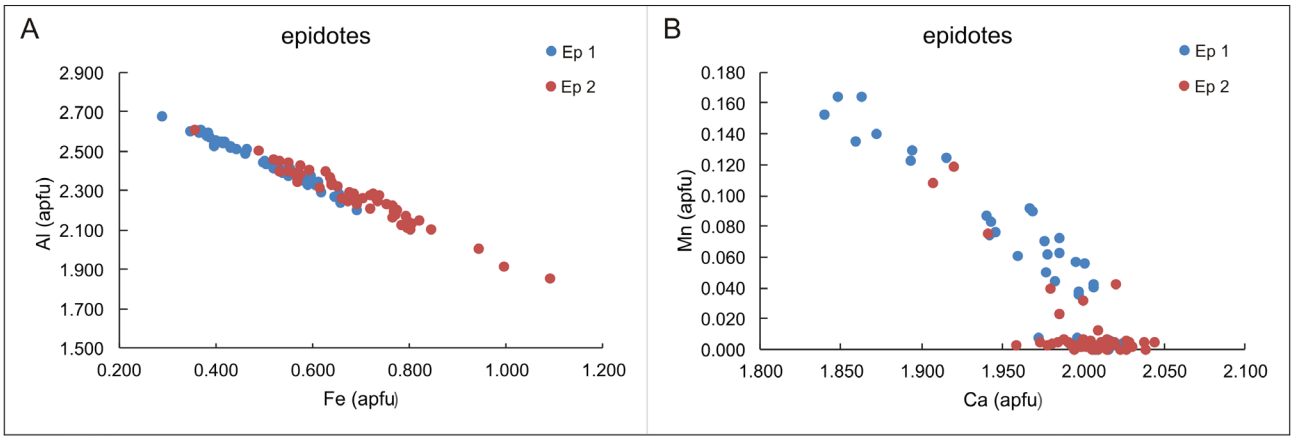

Fig. 9. Correlation between Al/Fe (**A**) and Ca/Mn (**B**) contents for both epidote generations.

than Mn^{3+} is expected (Bonazzi et al. 2009). The incorporation of Th^{4+} and U^{4+} in allanite is also observed at the *A* site. The usual ThO_2 content in natural allanites ranges between 2–3 wt% in contrast to UO_2, whose content is significantly lower (Gieré & Sorensen 2004 and references therein). The contents of ThO_2 (up to 3.68 wt%) and UO_2 (up to 0.19 wt%) in the Petrovitsa allanite, although increased, do not deviate significantly from normal values.

The incorporation of Cr and V in the crystal structure of allanite generally takes place at *M*-sites. Both elements could be present as major elements (Armbruster et al. 2006), but usually remain as trace constituents in epidote-group minerals. Comparative V and Cr enrichment in epidote minerals with respect to their host rocks has been commonly observed (Frei et al. 2004). The sources of V and Cr, as well as their behaviour, are generally different. Vanadium can be remobilised and incorporated into silicate minerals by metamorphosed organic matter, whereas Cr is usually related to magmatic processes or remobilisation after the destruction of pre-existing Cr-rich phases, or even a combination of both processes (Bačík & Uher 2010; Bačík et al. 2018 and references therein). The concentration of V in allanite from Petrovitsa pegmatites is mostly below 1000 ppm, whereas Cr_2O_3 reaches near 1.00 wt%. However, the enhanced contents of these elements are probably controlled by the fluid and host rock composition and interaction (e.g., the presence of amphibolite lenses near the pegmatite).

The incorporation of Ge is expected to take place at the expense of Si in the *T*-sites of the crystal structure, whereas Ga predominantly accommodates *M*-sites. Allanite samples enriched in Ge and Ga are described typically from sphalerite ore deposits (Frei et al. 2004), suggesting significant replacement of Si^{4+} by Ge^{4+} at *T*-sites and Al/Fe by Ga^{3+} at *M*-sites. Furthermore, extensive substitution for Si is favoured in REE-rich epidote minerals (Gieré & Sorensen 2004). The Petrovitsa pegmatites are injected into a high-grade metamorphic complex hosting significant Pb–Zn sulphide accumulation, which completely corresponds to the high contents of Ga and Ge in allanite. Since Pb–Zn mineralisation in the region is formed later, the incorporation of Ga and Ge may likely be the result of a late alteration of the mineral.

Most of the studied allanites are characterised by the relative depletion of REE and Th, including to a lesser extent Ti, Cr, and V, while at the same time, greater enrichment in Al and less Ca. This is likely due to the penetration and circulation of the multiphase post-pegmatite hydrothermal fluids and subsequent allanite alteration, leaching of the abovementioned elements, as well as the introduction of others. Therefore, allanite is transformed into an epidote-clinozoisite member. The released REE and Th from the accessory allanite are accumulated into the crystal structure of the later hydrothermal epidote, formed next to the allanite.

The complex textural zoning of the allanite suggests multiple growth stages and demonstrates additional indications of dissolution and recrystallisation resulting from repeated interactions of primary grains with late- to post-magmatic fluids, which produced a patchwork of domains of variable brightness as proposed by Petrík et al. (1995).

The increased content of Si, Al, and Ca in individual grains of allanite could also be explained by similar processes caused by late hydrothermal interaction. Furthermore, the alteration can be facilitated by the metamictisation degree of the mineral due to the radiogenic elements incorporated in the mineral structure (Gieré & Sorensen 2004).

In Table 2, it can be seen that the sum of the Si+P at the *T*-site is >3.05 *apfu*. According to Armbruster et al (2006), Si values >3.03 *apfu* may indicate either *A*-site vacancies or incomplete analyses. Based on our LA-ICP-MS data of the studied allanites, enhanced values of Pr and Sm are established, which were not measured in EPMA. This could possibly explain this considerable deviation. We did not perform normalisation of Si to 3.00 *apfu* because, according to Ercit (2002), this procedure can transfer all errors in Si determination to other cations in the formula, and therefore lead to potentially larger absolute errors.

Both epidote generations (Ep1 and Ep2) are the main hydrothermal alteration product which affected the pegmatites and results from a multiphase mineral formation during

Table 5: LA–ICP–MS representative analyses of both epidotes generations from the Petrovitsa deposit (ppm).

Type	epidote 1 pink						epidote 2 green					
Sample	Cl23 11	Cl23 12	Cl23 13	23-1 6	23-1 7	23-1 11	21 11	21 12	21 15	Cl23 5	Cl23 14b	23-3 9
Details	crystal 1			crystal 2	crystal 3	crystal 4	veinlet	veinlet	nest	veinlet	veinlet	nest
	rim	core	rim	next to aln	next to aln							
Li	bdl	bdl	bdl	bdl	bdl	bdl	bdl	bdl	bdl	1.53	0.52	bdl
B	17.58	22.73	21.23	35.27	23.35	22.64	108.08	110.75	56.95	17.48	29.91	56.38
V	61.29	68.19	85.03	16.16	4.48	5.28	58.81	91.56	3.04	27.25	22.22	40.33
Co	1.07	0.82	bdl	27.48	1.19	5.04	bdl	bdl	bdl	bdl	0.82	bdl
Ni	17.20	9.96	bdl	22.55	bdl	bdl	bdl	bdl	bdl	bdl	bdl	bdl
Zn	11.46	12.97	10.49	36.22	17.32	14.51	29.53	33.03	25.08	bdl	16.12	27.31
Ga	82.36	52.89	49.37	36.18	25.88	25.78	103.34	92.46	67.01	61.92	67.20	94.94
Ge	7.09	bdl	bdl	bdl	bdl	bdl	bdl	11.14	16.21	bdl	3.49	12.49
As	bdl	bdl	bdl	4.79	7.73	7.49	31.07	22.23	bdl	6.14	8.20	62.28
Rb	bdl	bdl	0.13	1.03	2.29	0.30	10.53	4.33	bdl	bdl	bdl	5.14
Sr	1225.17	1141.52	686.31	1617.39	1632.47	1504.19	842.89	956.59	1325.75	2263.69	765.69	900.40
Y	4.47	6.49	10.36	9.60	7.95	2.01	13.75	32.75	0.87	0.14	0.24	0.46
Zr	1.13	2.32	5.29	3.93	1.82	0.47	bdl	bdl	bdl	bdl	bdl	bdl
Nb	0.41	0.52	bdl	1.53	0.43	1.10	0.43	0.70	bdl	0.30	bdl	bdl
In	bdl	bdl	0.06	0.09	0.20	bdl	bdl	bdl	bdl	bdl	0.10	0.24
Sn	bdl	bdl	1.11	1.78	bdl	bdl	3.17	6.69	bdl	bdl	bdl	bdl
Sb	3.93	4.15	1.79	8.29	9.41	10.95	8.95	11.68	15.22	5.00	1.53	13.49
Cs	0.12	0.06	bdl	0.16	bdl	0.15	4.37	1.66	bdl	bdl	bdl	0.93
Ba	bdl	0.78	bdl	8.12	19.58	2.04	15.04	8.61	bdl	1.37	0.59	0.81
La	0.98	0.57	0.28	111.83	10.21	0.17	4.55	11.58	1.30	0.63	0.21	2.04
Ce	3.16	2.46	1.99	479.49	38.95	0.45	11.29	25.34	1.09	0.74	0.26	5.08
Pr	0.44	0.54	0.32	33.38	5.19	0.12	1.47	3.77	bdl	0.11	0.05	0.36
Nd	2.01	1.86	1.25	91.45	7.32	0.65	5.84	17.04	bdl	bdl	bdl	2.04
Sm	1.49	0.99	1.15	10.44	1.27	0.38	1.94	3.97	bdl	bdl	bdl	bdl
Eu	1.24	0.78	0.61	0.96	0.36	bdl	1.41	2.06	5.97	0.60	0.66	1.44
Gd	bdl	1.37	1.02	3.54	0.97	0.25	bdl	5.05	bdl	bdl	0.39	bdl
Tb	0.17	bdl	0.35	0.41	0.20	bdl	0.34	0.63	bdl	bdl	bdl	bdl
Dy	1.00	1.58	1.32	2.08	1.36	0.26	2.89	5.80	bdl	bdl	bdl	bdl
Ho	0.18	0.19	0.51	0.30	0.25	0.17	0.63	1.17	bdl	bdl	bdl	bdl
Er	0.34	bdl	2.34	0.70	0.50	0.30	bdl	4.48	bdl	bdl	bdl	bdl
Tm	bdl	0.16	0.23	bdl	0.12	0.06	0.26	0.71	bdl	bdl	bdl	bdl
Yb	bdl	0.62	1.27	bdl	0.49	0.23	2.48	5.11	bdl	bdl	bdl	bdl
Lu	bdl	0.12	0.25	bdl	bdl	bdl	bdl	0.60	bdl	bdl	bdl	bdl
Hf	bdl	bdl	bdl	0.21	0.47	<0.51681	bdl	bdl	bdl	bdl	bdl	bdl
Ta	0.11	0.21	bdl	0.19	0.29	0.24	0.28	bdl	bdl	0.30	0.07	bdl
W	bdl	bdl	bdl	0.76	0.88	0.63	bdl	bdl	bdl	bdl	bdl	12.27
Pb	10.25	14.04	5.90	46.69	38.85	31.46	31.58	28.56	40.09	20.37	6.67	35.54
Bi	0.10	bdl	0.13	0.28	bdl	bdl	bdl	0.37	bdl	1.30	0.49	0.71
Th	bdl	bdl	bdl	54.09	3.02	bdl	bdl	bdl	bdl	bdl	bdl	bdl
U	1.02	1.01	1.36	21.54	3.63	0.11	0.63	2.57	1.37	bdl	bdl	bdl

the extensive hydrothermal activity in the region. This mineralization is characterised by the low, but constant incorporation of Mn, which is related to the manganese geochemical specialisation of the hydrothermal mineralisation in the entire Madan region. Manganese-containing minerals from the epidote group, namely piemontite, are documented in the Laki and Davidkovo ore regions (Stoinova 1963; Marinova 1992).

Ep1 and Ep2 differ in morphology, colour, and chemical signatures. Ep1 is observed as dark to light pink crystals and shows distinct red-violet pleochroism, which according to Bonazzi & Menchetti (2004), is characteristic for manganian (i.e., Mn^{3+} bearing) epidote or clinozoisite, while manganoan (i.e., Mn^{2+} bearing) members do not exhibit the characteristic reddish hue. On the other hand, it is known that only low Mn^{3+} content is already sufficient to give pink colouring and piemontite-like pleochroism (Armbruster et al. 2006; Katerinopoulou et al. 2014). According to the recommended epidote-group nomenclature (Armbruster et al. 2006), Mn preferentially enters into the *M*-sites as Mn^{3+} and Mn^{2+}, as well as into *A*-sites as Mn^{2+}. When processing electron probe microanalyses, the assignment of the ionic species to the various key sites should begin with the infilling of the *T*-sites (mainly Si), followed by the octahedral *M*-sites (Al, Fe^{3+}, Mn^{3+}, V^{3+}, Cr^{3+}, Ti^{4+}, Sn^{4+}, Fe^{2+}, Mn^{2+}, Mg, etc.).

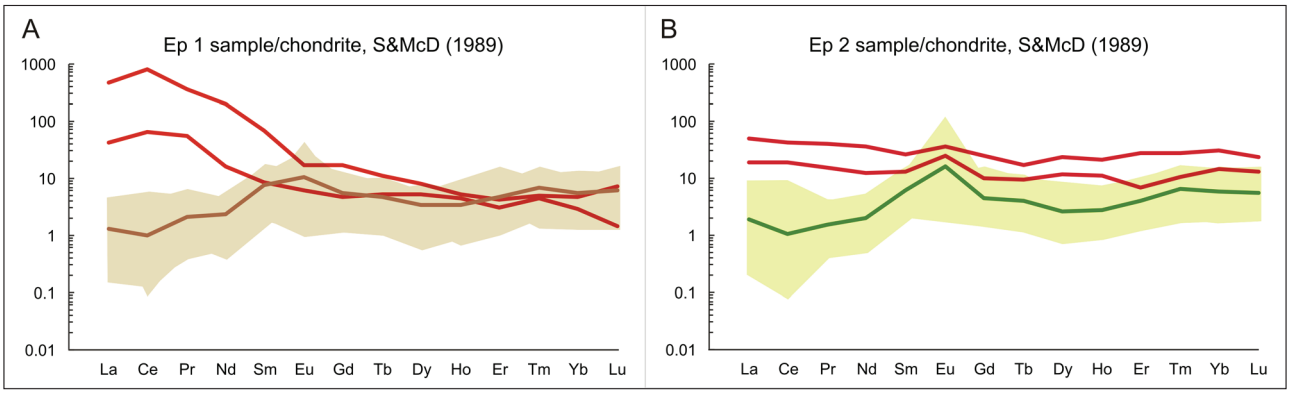

Fig. 10. Chondrite-normalised REE diagram for epidote 1 (**A**) and 2 (**B**) generations. The red lines demonstrate relatively high REE incorporation, which had been established in samples in close association with allanite or titanite. The shaded fields indicate range of values.

Finally, the *A*-sites should be accommodated, where priority must be given to Mn^{2+}. Considering epidote data from the present study, the majority of analyses from both generations reveal a deficit at the *M*-sites, while at the *A* sites, Ca reaches 2.00 *apfu*; therefore, Mn should be present either as Mn^{3+} and/or Mn^{2+} in the *M*-sites of the crystal structure. Only in a small number of analyses, a deficiency in both *M* and *A* sites suggests the assumption that Mn is redistributed among positions most likely as Mn^{3+} and Mn^{2+}. Based on the mineral relationships, the Ep1 is a product of the initial hydrothermal process, deposited in an Al- and Ca-rich environment with less Fe and Mn. Later, the hydrothermal fluids became enriched in Fe and Ep2 precipitates, followed by the base metal ore formation.

Conclusions

Epidote-group minerals are a major constituent in the pegmatites from the Petrovitsa deposit, developed as hydrothermal products occurring in an Al- and Ca-rich environment along the lithological contacts due to the interaction of pegmatite minerals with hot hydrothermal fluids. Apart from epidote-group minerals, the Ca-bearing mineral association includes hydrothermal titanite, carbonates, Ca-garnet, and skarn bustamite. According to the mineral relationships, the Ep1 is formed at the beginning of the hydrothermal process prior to the sulphide deposition. Initially, this epidote generation was developed at the expense of the feldspar (anorthite), which also resulted in the Al-dominated grain cores. Later, the hydrothermal fluid was enriched in Fe, resulting in Fe enrichment in Ep2 generation. Both hydrothermal epidote generations are defined as members of the clinozoisite–epidote series, reaching epidote members in the second generation. The minerals are formed within an oxidised environment indicated by Fe^{3+} incorporation. The REE contents in the studied epidotes are low except for some grains formed next to accessory allanite, where REE increase.

The accessory allanite-(Ce) crystallised under reducing conditions, as evident by the presence of Fe^{2+} in the structure. Most of the studied allanites suffered alteration due to the influx of multiphase hydrothermal events and are partly or entirely transformed to REE-rich epidote-clinozoisite, causing depletion in REE and Th and enrichment of Si, Al, and Ca. The alteration is a result of interaction between allanite and oxidized fluids causing considerable REE leaching from the mineral. Because of the limited mobility of REE in fluids, these elements are incorporated in closely crystalised epidotes.

Acknowledgments: The authors sincerely acknowledge the reviewers Jan Cempírek, Pavel Uher, and Peter Bačík for their very helpful critical comments and corrections that improved the manuscript. The study is financially supported by the Bulgarian National Science Fund KP-06-N34/4 project and complements ERA-MIN PEGMAT project KP-06-DO02/2.

References

Armbruster T., Bonazzi P., Akasaka M., Bermanec V., Chopin C., Giere R., Heuss-Assbichler S., Liebscher A., Menchetti S., Pan Y. & Pasero M. 2006: Recommended nomenclature of epidote-group minerals. *European Journal of Mineralogy* 18, 551–567. https://doi.org/10.1127/0935-1221/2006/0018-0551

Bonazzi P. & Menchetti S. 2004: Manganese in monoclinic members of the epidote group: piemontite and related minerals. *Reviews in Mineralogy and Geochemistry* 56, 495–552. https://doi.org/10.2138/gsrmg.56.1.495

Bonazzi P., Holtstam D., Bindi L., Nysten P. & Capitani G. 2009: Multi-analytical approach to solve the puzzle of an allanite-subgroup mineral from Kesebol, Västra Götaland, Sweden. *American Mineralogist* 94, 121–134. https://doi.org/10.2138/am.2009.2998

Dimov D., Dobrev S., Kolkovski B. & Sarov S. 2000: Structure, Alpine Evolution and Mineralizations of the Central Rhodopes Area (South Bulgaria). Guide to Excursion (B), ABCD–GEODE 2000 Workshop. *Sofia University*, Bulgaria, 1–50.

Dollase W.A. 1971: Refinement of the crystal structure of epidote, allanite and hancockite. *American Mineralogist* 56, 447–464.

Droop G.T.R. 1987: A general equation for estimating Fe^{3+} concentrations in ferromagnesian silicates and oxides from microprobe analyses, using stoichiometric criteria. *Mineralogical Magazine* 51, 431–435. https://doi.org/10.1180/minmag.1987.051.361.10

Ercit T.S. 2002: The mess that is "allanite". *Canadian Mineralogist* 40, 1411–1419. https://doi.org/10.2113/gscanmin.40.5.1411

Frei D., Liebscher A., Franz G. & Dulski P. 2004: Trace Element Geochemistry of Epidote Minerals. *Reviews in Mineralogy and Geochemistry* 56, 553–605. https://doi.org/10.2138/gsrmg.56.1.553

Georgieva S., Vassileva R., Milenkov G., Georgieva Y., Lutov G. & Stefanova E. 2020: Clinozoisite from the Petrovitsa Pb–Zn deposit, Madan region, Central Rhodopes. *Review of the Bulgarian geological society, Geosciences 2020*, 81, 37–39.

Georgieva S., Vassileva R., Milenkov G. & Stefanova E. 2021: Epidote-group minerals in altered pegmatites from Madan ore region, Central Rhodopes, Bulgaria: occurrence and chemistry. In: 9th International Conference Mineralogy and Museums, 24–26 August 2021, Sofia, Bulgaria, Extended abstracts. Sofia, 39–40.

Gieré R. & Sorensen S.S. 2004: Allanite and Other REE-Rich Epidote-Group Minerals. *Reviews in Mineralogy and Geochemistry* 56, 431–493. https://doi.org/10.2138/gsrmg.56.1.431

Gros K., Słaby E., Jokubauskas P., Sláma J. & Kozub-Budzyń G. 2020: Allanite Geochemical Response to Hydrothermal Alteration by Alkaline, Low-Temperature Fluids. *Minerals* 10, 392. https://doi.org/10.3390/min10050392

Hantsche A., Kouzmanov K., Milenkov G., Vezzoni S., Vassileva R., Dini A., Sheldrake T., Laurent O. & Guillong M. 2021: Metasomatism and cyclic skarn growth along lithological contacts: Physical and geochemical evidence from a distal Pb–Zn skarn. *Lithos* 400–401, 1–18. https://doi.org/10.1016/j.lithos.2021.106408

Ivanov Z. 2017: Tectonics of Bulgaria. *"St. Kliment Ohridski" University press*, Sofia, 1–332 (in Bulgarian).

Katerinopoulou A., Balic-Zunic T., Kolb J., Berger A. & Secher K. 2014: Manganiferous minerals of the epidote group from the Archaean basement of West Greenland. *Bulletin of the Geological Society of Denmark* 62, 27–37. https://boris.unibe.ch/id/eprint/69109

Marinova I. 1992: Geological position and mineralogical composition of the Belevsko deposit vein rhodonite mineralization, Davidkovo ore field. *Annual of Sofia University "St. Kliment Ohridski", Geology* 63, 139–157 (in Bulgarian with Russian and English abstracts).

Milenkov G., Vassileva R.D., Peytcheva I. & Grozdev V. 2020: U/Pb dating and trace element compositions in pegmatitehosted titanite from the Petrovitsa Pb-Zn deposit, Madan district, South Bulgaria. *Review of the Bulgarian geological society, Geosciences 2020*, 81, 90–92.

Milenkov G., Vassileva R.D., Georgieva S., Grozdev V. & Peytcheva I. 2022: Trace-element signatures and U–Pb geochronology of magmatic and hydrothermal titanites from Petrovitsa Pb–Zn deposit, Madan region, Central Rhodopes. *Geologica Balcanica,* in press.

Peterson R. & MacFarlane D. 1993: The rare-earth-element chemistry of allanite from the Grenville province. *Canadian Mineralogist* 31, 159–166.

Petrík I., Broska I., Lipka J. & Siman P. 1995: Granitoid Allanite-(Ce): Substitution Relations, Redox Conditions and REE Distributions (On An Example Of I-Type Granitoids, Western Carpathians, Slovakia). *Geologica Carpathica* 46, 79–94.

Poitrasson F. 2002: In situ investigations of allanite hydrothermal alteration: examples from calc-alkaline and anorogenic granites of Corsica (southeast France). *Contributions to Mineralogy and Petrology* 142, 485–500. https://doi.org/10.1007/s004100100303

Sarov S., Voynova E., Moskovski S., Jelezarski T., Naydenov K., Nikolov D., Georgieva I., Petrov N. & Markov N. 2006: Geological Map of the Republic of Bulgaria, Scale 1:50 000 Map Sheet K-35-86-Г (Madan). *Ministry of Environment and Water, Bulgarian National Geological Survey*, Sofia.

Stoinova M. 1963: Mineralogical stages in the Laky ore region. *Geochemistry, Mineralogy and Petrology* 6, 125–134 (in Bulgarian).

Sun S.-s. & McDonough W.F. 1989: Chemical and isotopic systematics of oceanic basalts: implications for mantle composition and processes. *Geological Society, London, Special Publications* 42, 313–345. https://doi.org/10.1144/GSL.SP.1989.042.01.19

Vassileva R.D. & Bonev I.K. 2003: Retrograde alterations of manganoan skarns in the Madan Pb–Zn deposits, South Bulgaria. In: Eliopoulos et al. (Eds.): Mineral Exploration and Sustainable Development. *Millpress*, Rotterdam, 403–406.

Vassileva R.D., Atanassova R. & Bonev I.K. 2009: A review of the morphological varieties of ore bodies in the Madan Pb–Zn deposits, Central Rhodopes, Bulgaria. *Geochemistry, Mineralogy and Petrology* 47, 31–49.

Vassileva R.D., Milenkov G. & Georgieva S. 2021: Pegmatites From The Pb–Zn Deposits In Central Rhodopes, South Bulgaria. In: Petrology and geodynamics of geological processes. *Proceedings of the XIII petrograpghic conference*, Irkutsk 3, 287–290.